Estimating Urban Growth from Landsat 8 Data Using Post-classification and Albedo Change Analysis in GEE Environment

Carlo Barletta, Alessandra Capolupo(✉), and Eufemia Tarantino

Department of Civil, Environmental, Land, Building Engineering and Chemistry (DICATECh), Politecnico di Bari, Via Orabona 4, 70125 Bari, Italy
{carlo.barletta,alessandra.capolupo,eufemia.tarantino}@poliba.it

Abstract. Urban growth, defined as the increase of artificial surfaces in cities or towns, is now considered critical for the environmental impacts it can generate. Mapping and monitoring the soil sealing phenomenon provides researchers, planners and decision-makers with useful information for sustainable development. Moreover, Earth observation remote sensing images, such as medium-resolution Landsat data, is widely adopted for short to long term urban change analysis. The aim of this paper is to extract information on land consumption occurred on urban areas (period 2015–2023) from Landsat 8 data using GEE cloud platform. The territory of the municipality of Bitritto, in Apulia region (Italy), was chosen as the study site. To achieve the objective of this work, a change detection approach, including both "post-classification comparison" and "image differencing" methods, was applied. To classify Landsat 8 multispectral images into a binary scheme ("urban areas" and "non-urban areas"), a decision tree approach using STRed and SwiRed indices, NIR/SWIR2 ratio and NIR band was developed and implemented in GEE environment. The "image differencing" step was, instead, performed by subtracting two land surface albedo maps, obtained from winter Landsat 8 images, for the two reference years. A neighborhood filter to remove isolated "changed" pixels was also applied to improve the outcome. The results were promising (P.A. 85% and U.A. 77% for the "urban growth" category, with an O.A. of 92%) even though some misclassifications were identified, probably due to "mixed" pixels or to some spectral confusion among certain land cover classes.

Keywords: Land consumption · Earth observation · change detection · soil sealing

1 Introduction

The urbanization process, which transforms natural landscapes into artificial areas, is recognized as one of the main drivers of land use and land cover (LU/LC) changes worldwide. The increase in man-made surfaces (such as rooftops, roads, parking lots, and so on) as a result of the construction of new buildings, transportation networks or other layers of totally or partly impermeable materials (i.e. concrete and asphalt) leads

© The Author(s), under exclusive license to Springer Nature Switzerland AG 2024
O. Gervasi et al. (Eds.): ICCSA 2024 Workshops, LNCS 14819, pp. 185–200, 2024.
https://doi.org/10.1007/978-3-031-65282-0_12

to the "soil sealing" phenomenon (understood as the covering of soil with impervious surfaces), which is now considered a serious environmental threat. Indeed, soil sealing affects several issues, including urban runoff, heat island effect, water and soil pollution, and biodiversity loss [1–5].

Detailed monitoring of LU/LC and urban growth provides valuable information for a sustainable land management. In particular, mapping the amount of impervious surfaces and detecting their changes over time through multi-temporal analyses helps planners, managers and researchers to understand urban patterns and processes and to assess the effectiveness of current policies in addressing the negative impacts of soil sealing.

Remote sensing data are well suited to acquire continuous information on the land surface at local, regional and global scales, and, also, over short to long time periods [1–6]. In addition, LU/LC changes can be detected and quantified from multi-date satellite observations that allow to measure the shift over time in biophysical variables such as the land surface albedo, which represents the proportion of solar radiation reflected from the Earth surface. For example, since more solar radiation is absorbed by vegetation, deforestation can be detected from albedo increase [7–12].

Various techniques have been developed over the years to perform change detection analyses from multi-temporal satellite images, including "image differencing", "image ratioing", "image classification and post-classification comparison", "change vector analysis", "image regression", and so on [6]. "Image differencing" and "image ratioing" between multi-temporal images are effective for a quick and quantitative assessment of changes but are limited by the difficulties in interpreting different type of LU/LC transformation characterized by similar reflectance change. "Image classification and post-classification comparison", consisting, instead, in comparing multi-date LU/LC classified maps on a pixel-by-pixel basis, is a simple, effective, and very used method but it suffers from the error propagation from the independently classified maps. "Change vector analysis" measures the magnitude and direction of change but it is challenged by multi-temporal illumination differences and the presence of noise in the result. Lastly, "image regression" method can provide better results than simple "image differencing"; however, its application suffers from non-stationary relationships (typical in geographical data) in the spatial structure of data [6, 13, 14].

These techniques have been largely tested on satellite images provided by multispectral platforms. However, Landsat mission appears as an optimal solution to address such issues since it is the only source of free images acquired in more than 50 years with a geometric, spectral and temporal resolution adapt for urban analysis. Hence, Landsat multi-decadal observations of the Earth surface are among the most suitable for short to long-term analysis of environmental and land changes like, for example, forest cover and biodiversity changes, or the expansion of urban areas [3, 6, 15–18].

The rise of geospatial big data in recent years leads to different challenges such as difficulties in their acquisition, storage, visualization, processing and analysis. To overcome these problems, cloud-based platform, such as Google Earth Engine (GEE), have been introduced to speed up the operations and provide better access to the data [3, 7, 19–22].

The objective of this research is to quantify the expansion of urban areas using Landsat 8 (L8) satellite data from 2015 to 2023. This is achieved through the development

of a hierarchical model integrating the index-based method for LU/LC extraction and albedo change analysis. A custom JavaScript code was created and implemented within the GEE platform to facilitate this analysis. The municipality of Bitritto, located in southern Italy, was selected as the pilot site for testing such a methodology.

2 Materials and Methods

This section describes the materials and methods used in this research. Moreover, Sect. 2.1 briefly introduces the study area of Bitritto, while Sect. 2.2 provides information on the GEE cloud platform and the satellite data selected. Subsequently, Sects. 2.3, 2.4 and 2.5 present, respectively, the LU/LC classification and post-classification comparison phase, the image differencing and isolated pixel phase, and the algorithm for the land surface albedo estimation. Lastly, in Sect. 2.6 is described the method for the accuracy assessment of the urban change map.

To accomplish the objective of this study, a combined approach using two widely recognized change detection methods "image classification and post-classification comparison" and "image differencing" was employed. The proposed methodology consists of four main steps:

- initially, cloud-free L8 images for each reference year underwent classification. This classification involved a hierarchical method involving SwirTirRed (STRed) and SwiRed indices, near infrared (NIR)/shortwave infrared band 2 (SWIR2) ratio, and the NIR band;
- subsequently, the resulting classified maps underwent a pixel-by-pixel comparison;
- areas identified as potential changes from "non-urban" to "urban" underwent further analysis using the "image differencing" method. This entailed comparing two land surface albedo maps, derived from single 2015 and 2023 winter L8 images. To enhance accuracy, appropriate thresholds were established to eliminate false "changed" pixels;
- lastly, a filtering process was implemented on the final "urban change map" to eliminate isolated "changed" pixels and refine the results.

This methodological approach integrates both classification and change detection techniques, offering a comprehensive analysis of urban growth dynamics over time. This approach is synthetically represented in Fig. 1.

After collecting the L8 Surface Reflectance (SR) and raw satellite images dated 29 August 2015 and 19 August 2023 from the GEE data catalogue, the LU/LC maps were obtained using the decision tree algorithm detailed in Sect. 2.4.

The extracted classes were then aggregated in binary maps to delineate "urban" and "non-urban" areas and, the "post-classification comparison" method was applied. Subsequently, the "image differencing" method was applied to the resulting potential "changed" pixels (transitioning from "non-urban" to "urban") to refine change detection, thereby eliminating false "changed" areas attributed to misclassifications present in the 2015 and 2023 LU/LC maps.

To this purpose, two winter Top-Of-Atmosphere (TOA) L8 images, acquired on 18 February 2015 and 24 February 2023, were used to retrieve the land surface albedo

maps. Therefore, after subtracting the 2015 from 2023 albedo maps and defining an appropriate threshold representing significant changes in LU/LC, this phase effectively identified and removed several false "changed" areas.

Lastly, a filter to remove isolated pixels was applied to improve the final change map.

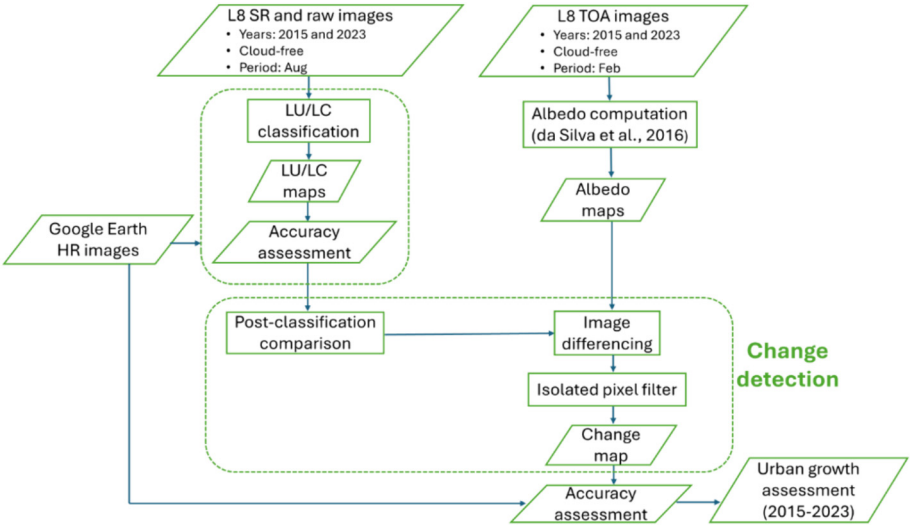

Fig. 1. Workflow. HR: High-resolution.

2.1 Study Area

The territory of the municipality of Bitritto (Fig. 2), in southern Italy, was selected as study site. This area of about 18 km^2, part of the Metropolitan City of Bari, in the center of the Apulia region, is characterized by a mainly flat topography and a land cover with a high proportion of agricultural fields or other green spaces and a relatively low proportion of built-up land. Nevertheless, like many other areas in the region, it has experienced significant land consumption in recent decades. The climate of Bitritto is Mediterranean, with hot and dry summers and mild winters [25–27].

2.2 GEE Platform and Input Data

The present work was carried out in GEE cloud platform. GEE consists of a high-performance computing service connected with a multi-petabyte data catalog of Earth observation imagery (including Landsat raw and preprocessed data), with an interactive environment for rapidly storing, managing and processing a large volume of geospatial data. The available Application Programming Interfaces (APIs) are JavaScript and Python [7, 19, 21–23]. In particular, the JavaScript interface was chosen for this study.

Table 1 highlights the data selected for this study. Cloud-free SR and raw L8 satellite images, for the reference years 2015 and 2023, acquired in the summer period,

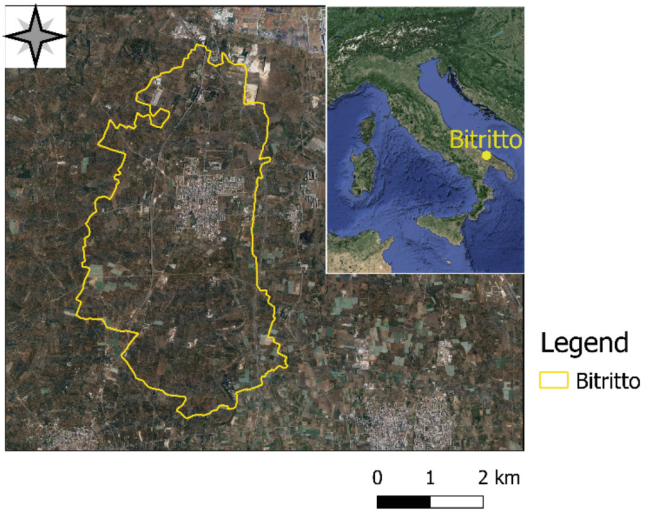

Fig. 2. Study area.

were selected from the GEE data catalogue. These images were used for the LU/LC classification of the study site, as elaborated upon in subsequent sections.

Moreover, the analysis of two additional high-resolution images available in Google Earth Pro [28], encompassing the study area and acquired on 29 August 2015 and 27 April 2023, respectively, proved beneficial for selecting training and testing pixels for the LU/LC classification, as well as for the accuracy assessment of the maps.

Finally, one TOA winter L8 image was selected for each reference year to compute land surface albedo maps. These maps were then used for the "image differencing" change detection phase, as discussed in Sect. 2.5.

Table 1. Selected data. HR: High Resolution.

ID	Data	Period	Phase
1	L8 SR and raw images	29 Aug 2015	LU/LC classification
2	L8 SR and raw images	19 Aug 2023	LU/LC classification
3	Google Earth HR image	29 Aug 2015	Training stage and validation
4	Google Earth HR image	27 Apr 2023	Training stage and validation
5	L8 TOA image	18 Feb 2015	Albedo computation
6	L8 TOA image	24 Feb 2023	Albedo computation

2.3 Image Classification and Post-classification Comparison

In this study, a decision tree LU/LC classification was developed and implemented in GEE cloud environment by writing a proper JavaScript code.

The chosen classification scheme includes four LU/LC categories to be discriminated: "vegetation", "plastic greenhouses", "urban areas" and "bare soil".

The method proposed (Fig. 3) implies the sequential application of three binary decision rules including the STRed and SwiRed spectral indices (developed for the Landsat Image Classification Algorithm [LICA] in 2020 [23]), the NIR/SWIR2 ratio and the NIR band. Therefore, the LU/LC classes were distinguished in the following order: 1) "vegetation" (using STRed, SwiRed and NIR band), 2) "plastic greenhouses" (using NIR/SWIR2 ratio and NIR band), and 3) "urban areas" and "bare soil" (using SwiRed).

The STRed and SwiRed indices are expressed as follows:

$$STRed = \frac{SWIR1 + Red - TIR1}{SWIR1 + Red + TIR1}, \tag{1}$$

$$SwiRed = \frac{SWIR1 - Red}{SWIR1 + Red} \tag{2}$$

where SWIR1, Red and TIR1 are Landsat shortwave infrared band 1, red band and thermal infrared band 1, respectively [23].

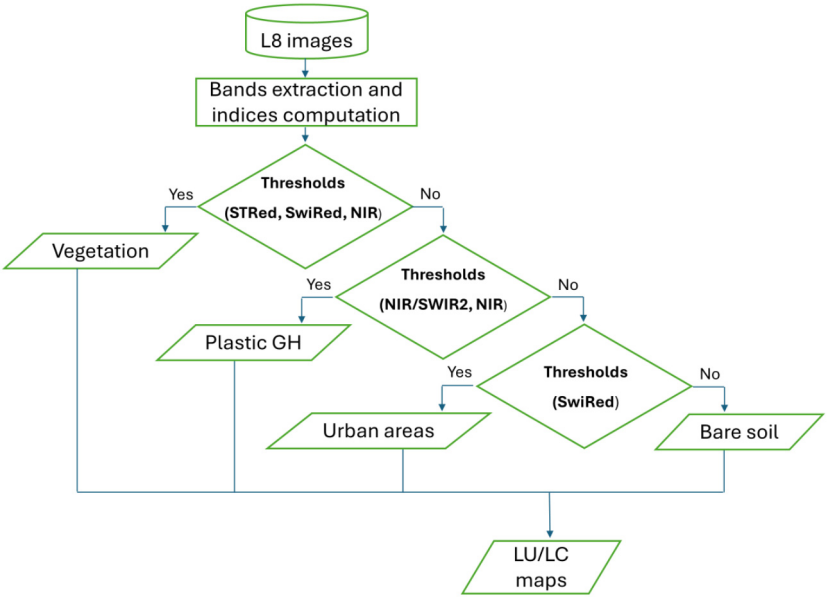

Fig. 3. Flowchart of the algorithm for the LU/LC classification.

A consistent number of training pixels for each of the four LU/LC categories were selected on Landsat 8 SR images. The visualization of Google Earth high-resolution

images, available in Google Earth Pro [28], was very useful to correctly distinguish each category on the ground.

Average spectral signature plots (Fig. 4) were then retrieved in the GEE platform:

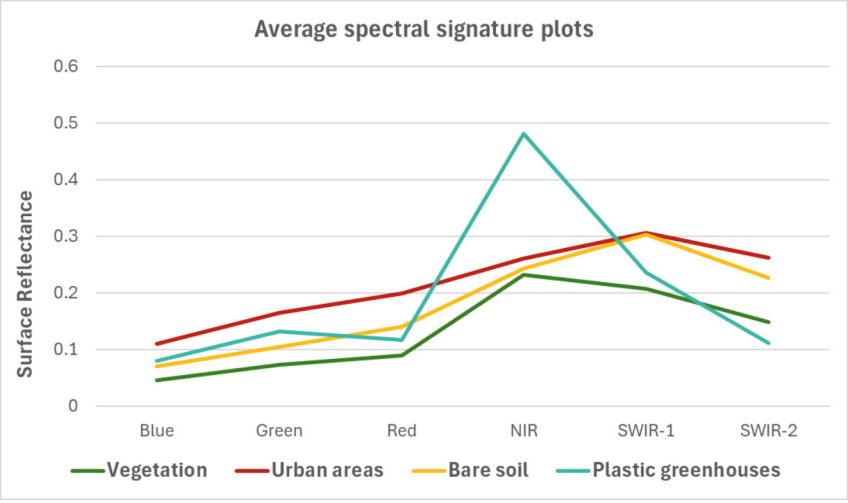

Fig. 4. Average spectral signature plots for training pixels of "vegetation", "urban areas", "bare soil" and "plastic greenhouses" categories obtained from Landsat 8 SR images for the study area of Bitritto.

A scatter diagram between STRed and SwiRed indices (Fig. 5) was obtained to analyze the separability of the four thematic classes and to choose suitable thresholds for the decision rules. This analysis suggested the selection of SwiRed thresholds (used in LICA [23] only for extracting built-up areas) to better discriminate the "vegetation" class (including both sparse and dense vegetated areas) from other categories, in addition to the STRed index (already adopted in LICA [23] for the vegetation extraction).

Moreover, in order to extract the "plastic greenhouses", the analysis of Fig. 4 suggested that the NIR and SWIR2 bands could be the most suitable for identifying them with a good accuracy, due to the relative reversal of their spectral response for these bands compared to those of the other three classes. The scatter diagram between NIR and SWIR2 confirmed this hypothesis, as shown in Fig. 6, where the spectral separability of plastics from the other categories is very evident.

Therefore, thresholds of NIR and NIR/SWIR2 ratio from Landsat 8 SR images were set to extract the "plastic greenhouses" LU/LC category.

After distinguishing "vegetation" and "plastic greenhouses", the SwiRed index was applied on Landsat 8 SR images to discriminate the "urban areas" class (including the LICA "built-up" and "mining areas" categories). Finally, the remaining part of the images was classified as "bare soil".

The resulting classified maps were then aggregated into a binary map containing only "urban areas" and "non-urban areas" categories (the latter resulting from the aggregation

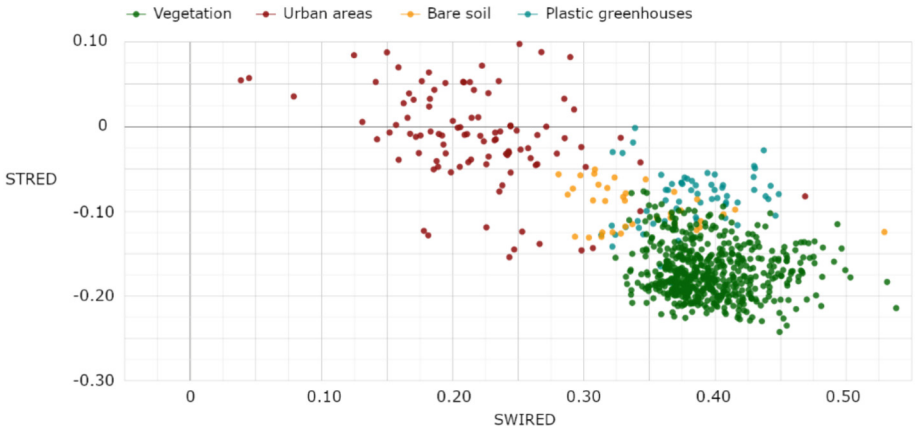

Fig. 5. Scatter diagram (STRed/SwiRed) for training pixels of "vegetation", "urban areas", "bare soil" and "plastic greenhouses" categories obtained from Landsat 8 SR images for the study area of Bitritto.

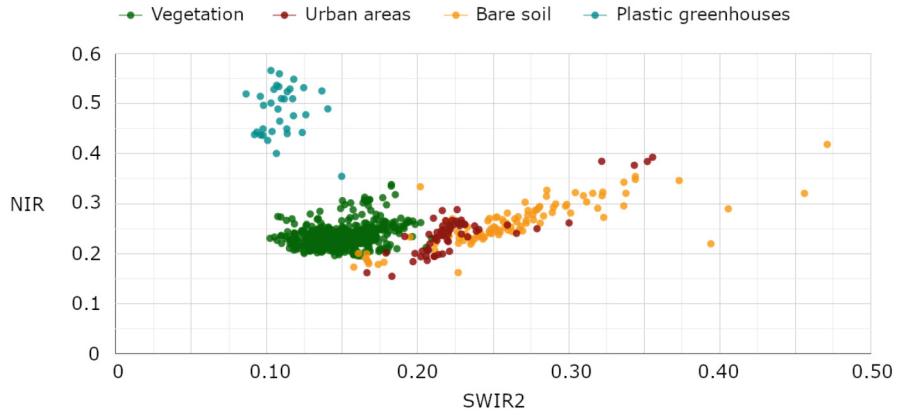

Fig. 6. Scatter diagrams (NIR/SWIR2) for training pixels of "vegetation", "urban areas", "bare soil" and "plastic greenhouses" categories obtained from Landsat 8 SR images for the study area of Bitritto.

of "vegetation", "plastic greenhouses" and "bare soil"), in order to perform the change detection and the evaluation of the urban growth (2015–2023).

After aggregating the 2015 and 2023 LU/LC maps into a binary classification scheme ("urban areas" and "non-urban areas"), the two resulting maps (the "soil sealing maps") were compared pixel-by-pixel. In this way, the possible outcomes were "no change" (in case of the same classification in both 2015 and 2023 maps) or "change" (for pixels classified differently in 2015 and in the 2023 map).

2.4 Image Differencing and Isolated Pixel Filter

After the post-classification comparison, for the resulting "changed" pixels (specifically, for pixels changed from "non-urban" in 2015 to "urban" in 2023), the "image differencing" method was applied calculating the difference images between the two land surface albedo maps, estimated from single cloud-free L8 TOA winter images (acquired on 18 February 2015 and on 24 February, respectively, for the reference years 2015 and 2023). A suitable threshold of albedo change, possibly representative of significant LU/LC changes, from "non-urban" to "urban", was found. Late winter imagery was preferred over other seasons because changes from bare or sparsely vegetated land to built-up areas may be most apparent due to the higher moisture content and green cover (resulting in lower albedo value) of the former in this season, since higher rainfall during the autumn/winter period is typical for the climate of the study area [26, 33–39]. Therefore, an increase in albedo, from 2015 to 2023 images, could be a sign of a land cover transformation from non-artificialized land to urbanized land (urban growth) [40–42].

After the "image differencing" phase, a connected neighbors filter to remove isolated "changed" pixels was implemented in GEE to further clean the change map from remaining misclassifications, and to obtain the "urban change map" (2015–2023), representing two categories: "urban growth" and "no growth".

2.5 Albedo Estimation

The land surface albedo maps were retrieved by applying the da Silva et al. algorithm (2016) [24], developed specifically for Landsat 8 data, expressed as follows:

$$\alpha = \frac{(\alpha_{TOA} - \alpha_{ATM})}{\tau^2} \tag{3}$$

where α_{TOA} is the TOA albedo, computed on Landsat 8 TOA reflectances, α_{ATM} is the atmospheric albedo, which was set equal to 0.03 as discussed in [19], and τ^2 is the square of the atmospheric transmissivity for shortwave radiation [19, 24, 33, 43]. The value of α_{TOA} is calculated with the following equation:

$$\alpha_{TOA} = p_2 * Blue + p_3 * Green + p_4 * Red + p_5 * NIR + p_6 * SWIR1 + p_7 * SWIR2 \tag{4}$$

where p_i are weighting coefficients [24, 33].

2.6 Accuracy Assessment of the Urban Change Map

To evaluate the accuracies of the classified maps, a multi-temporal dataset of test pixels was generated using the stratified random sampling method. A total number of 245 "pure" pixels were selected, according to the extent of each class, in the following proportions: 140 for "vegetation", 55 for "urban areas", 30 for "bare soil" and 20 for "plastic greenhouses". A visual interpretation of the high-resolution Google Earth images, chosen as "reference" data, was performed to assign each sample pixel to the correct category, based on its location. The metrics calculated to assess the accuracy were overall accuracy (O.A.), producer accuracy (P.A.), and user accuracy (U.A.) [19, 25–28].

To evaluate the accuracy of the change map, which shows the land consumption occurred in Bitritto for the period 2015–2023, a dataset of 100 test pixels, representing "urban growth" and "no growth", was obtained with the stratified random sampling method, after the visual interpretation of the multitemporal high-resolution Google Earth images [28]. According to the extent of each class, the pixels were selected in the following proportions: 20 for "urban growth" category, and 80 for "no growth" class. The metrics calculated to evaluate the accuracy were O.A., P.A. and U.A.

3 Results and Discussion

In this section, Sect. 3.1 presents and discusses the results of the LU/LC classification obtained from the decision tree approach described in Sect. 2, while Sect. 3.2 presents and discusses the results of the change detection method applied to extract the urban growth map (2015–2023) for the Bitritto study area.

3.1 LU/LC Classification Maps and Accuracy Assessment

The LU/LC maps, retrieved for the years 2015 and 2023 in GEE after applying the method described in Sect. 2.4, are shown in Fig. 7. The accuracy metrics, instead, obtained for the validation of the thematic maps, are reported in Table 2.

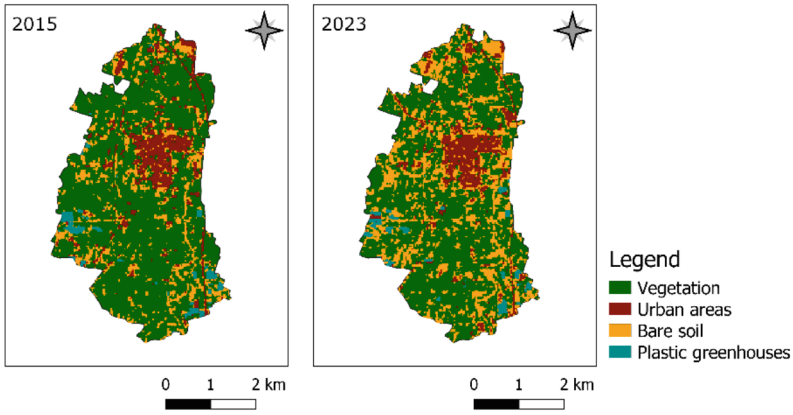

Fig. 7. LU/LC maps of 2015 and 2023 for the study area.

The analysis of the accuracy metrics highlights that the O.A. was quite high for both classification maps (about 90%), while plastic greenhouses and vegetation were those classes with both O.A. and U.A. higher than 90%. The extraction of urban areas was very good with P.A. accuracies of 85% and 84% for 2015 and 2023, respectively, while the U.A. accuracies were very high totaling 98% in 2015 maps and 96% for the 2023 classification. Lower accuracies characterize, instead, the bare soil extraction (P.A. $>$ 70% and U.A. $>$ 55%).

Table 2. Accuracy metrics for the LU/LC maps.

	2015		2023	
LU/LC class	P.A. [%]	U.A. [%]	P.A. [%]	U.A. [%]
Vegetation	95	92	93	94
Urban areas	85	98	84	96
Bare soil	70	64	73	56
Plastic greenhouses	100	100	95	100
O.A. [%]	90		89	

3.2 Change Detection

The 2015 and 2023 LU/LC maps were subsequently aggregated into a binary classification (where the two classes are: "non-urban areas" including vegetation, bare soil and plastic greenhouses, and "urban areas"). The "soil sealing maps" obtained after this aggregation are shown in Fig. 8. The visual analysis of these outcomes suggests that, probably, only little changes occurred in the period 2015–2023.

To estimate the urban growth, a "post-classification" comparison change detection was first performed between these maps. Since some misclassifications are present in both outcomes, this step was not sufficient to detect the land consumption with a good accuracy. Therefore, a second step ("image differencing" between two albedo maps retrieved from winter images, as explained in Sect. 2.5), and a third step consisting in a filter of isolated "changed" pixels, was necessary.

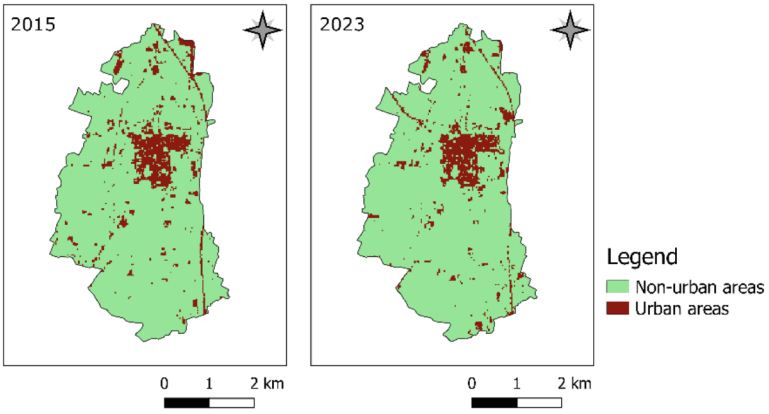

Fig. 8. Soil sealing maps of 2015 and 2023 for the study area.

Figure 9 show the land surface albedo maps retrieved by applying the da Silva et al. (2016) algorithm [24].

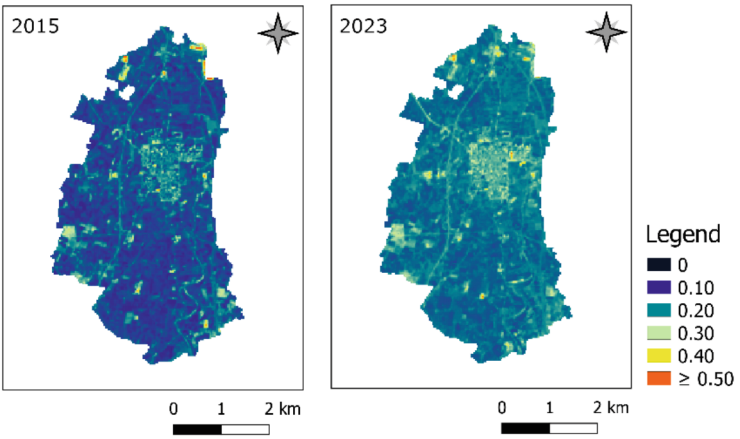

Fig. 9. Land surface albedo maps of 2015 and 2023 for the study area.

These two images were subtracted in the GEE platform, and an albedo increase greater than 0.055 between 2015 and 2023 was selected as the threshold for the urban growth detection.

Finally, a filter to eliminate isolated changed pixels were applied to further improve the outcome.

The final "urban change map", obtained using the change detection approach described above, is shown in Fig. 10, while the accuracy metrics for the change map are reported in Table 3.

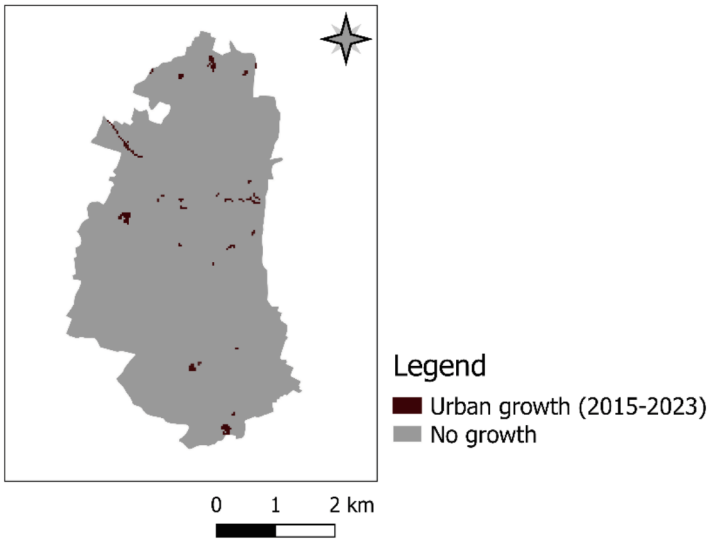

Fig. 10. Urban change map 2015–2023 for the study area.

Table 3. Accuracy metrics for the urban change map.

	2015–2023	
Class	P.A. [%]	U.A. [%]
Urban growth	85	77
No growth	94	96
O.A. [%]	92	

From Table 3 it can be noticed that the O.A. for the urban change map was high (92%). Regarding the estimation of the "urban growth" (2015–2023), satisfactory results were found, with a P.A. of 85% and a U.A. of 77%. Moreover, the analysis of the map confirms that the land consumption for the Bitritto study area is moderate for the period 2015–2023. However, a few mis-changed areas are still present in the map, probably due to the "mixed" pixels issue (typical for the classification of medium-resolution images [2, 44], such as Landsat data) or to the little spectral confusion that persists among certain classes (in particular, between "urban areas" and "bare soil").

The methodology proposed in this study, developed for free and open medium-resolution Landsat satellite data, provided, therefore, promising results in terms of automatically extracting information on land consumption occurring at the urban scale. The high values of the accuracy metrics, obtained for the change map, suggest that it could be reasonably applied in the future to contribute, thanks to its relative simplicity and feasibility, to the rapid monitoring of urban development and the soil sealing phenomenon, both at regional and local levels.

4 Conclusion

The increase in artificialized surfaces caused by urbanization has a direct impact on many environmental issues (i.e., the soil sealing phenomenon) [1, 4, 5, 27, 44].

Remote sensing data are very useful for mapping impervious surfaces and estimating urban growth using various techniques [4, 6]. In particular, Landsat medium-resolution multispectral imagery has been widely adopted to identify land cover transformations, such as detecting the expansion of artificial areas [15, 16, 19, 45, 46].

In this work, it has been possible to extract land consumption information for the study territory of Bitritto, in the central Apulia region (Italy), from 2015 to 2023, where a moderate soil consumption was found to have occurred during the period considered.

A combined approach between a "post-classification comparison" among two LU/LC maps (obtained through an index-based decision tree approach) and the "image differencing" of late winter albedo maps, retrieved from Landsat 8 data, provided satisfactory results in terms of accuracy of the urban growth map.

Furthermore, the GEE platform, used in this study to minimize the acquisition and operational time required for satellite image processing (thanks to cloud technology), was confirmed to be optimal for analyzing and monitoring the evolution of land surface features [7, 47, 48].

Disclosure of Interests. The authors have no competing interests to declare that are relevant to the content of this article.

References

1. Peroni, F., et al.: How to map soil sealing, land take and impervious surfaces? A systematic review. Environ. Res. Lett. **17**(5), 053005 (2022)
2. Wang, Y., Li, M.: Urban impervious surface detection from remote sensing images: a review of the methods and challenges. IEEE Geosci. Remote Sens. Mag. **7**(3), 64–93 (2019)
3. Kabisch, N., Selsam, P., Kirsten, T., Lausch, A., Bumberger, J.: A multi-sensor and multi-temporal remote sensing approach to detect land cover change dynamics in heterogeneous urban landscapes. Ecol. Ind. **99**, 273–282 (2019)
4. Weng, Q. (Ed.): Remote Sensing of Impervious Surfaces. CRC Press (2007)
5. Valera Lozano, A., Añóvidal, C., Sánchez Díaz, J.: Urban growth (1956–2012) and soil sealing in the metropolitan area of Valencia (Eastern Spain). Spanish J. Soil Sci. **9**(2), 88–104 (2019)
6. Bhatta, B.: Analysis of Urban Growth and Sprawl from Remote Sensing Data. Springer, Heidelberg (2010). https://doi.org/10.1007/978-3-642-05299-6
7. Capolupo, A., Monterisi, C., Sonnessa, A., Caporusso, G., Tarantino, E.: Modeling land cover impact on albedo changes in Google earth engine environment. In: Gervasi, O., et al. (eds.) International Conference of Computational Science and Its Applications, LNCS, vol. 12955, pp. 89–101. Springer, Cham (2021). https://doi.org/10.1007/978-3-030-87007-2_7
8. Münch, Z., Gibson, L., Palmer, A.: Monitoring effects of land cover change on biophysical drivers in rangelands using albedo. Land **8**(2), 33 (2019)
9. Cunha, J., Nóbrega, R.L.B., Rufino, I., Erasmi, S., Galvão, C., Valente, F.: Surface albedo as a proxy for land-cover clearing in seasonally dry forests: evidence from the Brazilian Caatinga. Remote Sens. Environ. **238**, 111250 (2020)
10. Berbet, M.L., Costa, M.H.: Climate change after tropical deforestation: seasonal variability of surface albedo and its effects on precipitation change. J. Clim. **16**(12), 2099–2104 (2003)
11. Houspanossian, J., Giménez, R., Jobbágy, E., Nosetto, M.: Surface albedo raise in the south American Chaco: combined effects of deforestation and agricultural changes. Agric. For. Meteorol. **232**, 118–127 (2017)
12. Polykretis, C., Grillakis, M.G., Alexakis, D.D.: Exploring the impact of various spectral indices on land cover change detection using change vector analysis: a case study of Crete Island Greece. Remote Sens. **12**(2), 319 (2020)
13. Ridd, M.K., Liu, J.J.: A comparison of four algorithms for change detection in an urban environment. Remote Sens. Environ. **63**, 95–100 (1998)
14. Hardin, P.J., Jackson, M.W., Otterstrom, S.M.: Mapping, measuring, and modeling urban growth. In: Jensen, R.R., Gatrell, J.D., McLean, D. (eds.) Geo-Spatial Technologies in Urban Environments, 2nd edn., pp. 141–176. Springer, Berlin (2007). https://doi.org/10.1007/978-3-540-69417-5_8
15. Wulder, M.A., et al.: Fifty years of Landsat science and impacts. Remote Sens. Environ. **280**, 113195 (2022)
16. Wulder, M.A., et al.: Current status of Landsat program, science, and applications. Remote Sens. Environ. **225**, 127–147 (2019)
17. Totaro, V., Gioia, A., Novelli, A., Caradonna, G.: The use of geomorphological descriptors and Landsat-8 spectral indices data for flood areas evaluation: a case study of Lato river basin. In: Gervasi, O., et al. (eds.) International Conference of Computational Science and Its Applications, LNCS, vol. 10407, pp. 30–44. Springer, Cham. (2017). https://doi.org/10.1007/978-3-319-62401-3_3

18. Totaro, V., Peschechera, G., Gioia, A., Iacobellis, V., Fratino, U.: Comparison of satellite and geomorphic indices for flooded areas detection in a Mediterranean river basin. In: Misra, S., et al. (eds.) International Conference of Computational Science and Its Applications, LNCS, vol. 11622, pp. 173–185. Springer, Cham. (2019). https://doi.org/10.1007/978-3-030-24305-0_14
19. Barletta, C., Capolupo, A., Tarantino, E.: Extracting land surface albedo from Landsat 9 data in GEE platform to support climate change analysis. Geomat. Environ. Eng. **17**(6), 35–75 (2023)
20. Novelli, A., Tarantino, E., Caradonna, G., Apollonio, C., Balacco, G., Piccinni, F.: Improving the ANN classification accuracy of landsat data through spectral indices and linear transformations (PCA and TCT) aimed at LU/LC monitoring of a river basin. In: Gervasi, O., et al. (eds.) International Conference of Computational Science and Its Applications, LNCS, vol. 9787, pp. 420–432. Springer, Cham. (2016). https://doi.org/10.1007/978-3-319-42108-7_32
21. Gorelick, N., Hancher, M., Dixon, M., Ilyushchenko, S., Thau, D., Moore, R.: Google earth engine: planetary-scale geospatial analysis for everyone. Remote Sens. Environ. **202**, 18–27 (2017)
22. Tamiminia, H., Salehi, B., Mahdianpari, M., Quackenbush, L., Adeli, S., Brisco, B.: Google earth engine for geo-big data applications: a meta-analysis and systematic review. ISPRS J. Photogramm. Remote Sens. **164**, 152–170 (2020)
23. Capolupo, A., Monterisi, C., Tarantino, E.: Landsat images classification algorithm (LICA) to automatically extract land cover information in Google earth engine environment. Remote Sens. **12**(7), 1201 (2020)
24. da Silva, B.B., Braga, A.C., Braga, C.C., de Oliveira, L.M.M., Montenegro, S.M.G.L., Barbosa Junior, B.: Procedures for calculation of the albedo with OLI-Landsat 8 images: application to the Brazilian semi-arid. Revista Brasileira de Engenharia Agricola e Ambiental **20**(1), 3–8 (2016)
25. Labadessa, R., Ancillotto, L.: Small but irreplaceable: The conservation value of landscape remnants for urban plant diversity. J. Environ. Manage. **339**, 117907 (2023)
26. Autorità di Bacino della Puglia: Piano di Bacino Stralcio dell'Assetto Idrogeologico (PAI) (2004)
27. Munafò, M. (Ed.): Consumo di suolo, dinamiche territoriali e servizi ecosistemici. Report SNPA 32 (2022)
28. Google Earth Pro. https://www.google.com/intl/it/earth/about/versions/#earth-pro. Accessed 28 February 2024
29. Congalton, R.G.: A review of assessing the accuracy of classifications of remotely sensed data. Remote Sens. Environ. **37**(1), 35–46 (1991)
30. Congalton, R.G.: Accuracy assessment and validation of remotely sensed and other spatial information. Int. J. Wildland Fire **10**(4), 321–328 (2001)
31. Brivio, P., Lechi, G., Zilioli, E. (2006). Principi e metodi di telerilevamento. CittaStudi (2006)
32. Crocetto, N., Tarantino, E.: A class-oriented strategy for features extraction from multidate ASTER imagery. Remote Sens. **1**(4), 1171–1189 (2009)
33. Barletta, C., Capolupo, A., Tarantino, E.: Exploring the potentialities of Landsat 8 and sentinel-2 satellite data for estimating the land surface albedo in urban areas using GEE platform. In: Gervasi, O., et al. (eds.) International Conference on Computational Science and Its Applications, LNCS, vol. 13379, pp. 435–449. Springer, Cham. (2022). https://doi.org/10.1007/978-3-031-10545-6_30
34. Polemio, M., Lonigro, T.: Trends in climate, short-duration rainfall, and damaging hydrogeological events (Apulia, Southern Italy). Nat. Hazards **75**(1), 515–540 (2015)
35. Cotecchia, V., Simeone, V., Gabriele, S.: Caratteri climatici. In: Acque sotterranee e l'intrusione marina in Puglia: dalla ricerca all'emergenza nella salvaguardia della risorsa.

Memorie descrittive della carta geologica d'Italia 92, pp. 338–369. ISPRA Serv. Geologico d'Italia (2014)
36. Guan, X., Huang, J., Guo, N., Bi, J., Wang, G.: Variability of soil moisture and its relationship with surface albedo and soil thermal parameters over the Loess Plateau. Adv. Atmos. Sci. **26**, 692–700 (2009)
37. Sanchez-Mejia, Z.M., Papuga, S.A., Swetish, J.B., van Leeuwen, W.J.D., Szutu, D., Hartfield, K.: Quantifying the influence of deep soil moisture on ecosystem albedo: the role of vegetation. Water Resour. Res. **50**(5), 4038–4053 (2014)
38. Yang, J., Li, Z., Zhai, P., Zhao, Y., Gao, X.: The influence of soil moisture and solar altitude on surface spectral albedo in arid area. Environ. Res. Lett. **15**(3), 035010 (2020)
39. Liu, S., Chadwick, O.A., Roberts, D.A., Still, C.J.: Relationships between GPP, satellite measures of greenness and canopy water content with soil moisture in Mediterranean-climate grassland and oak savanna. Appl. Environ. Soil Sci. **2011** (2011)
40. de Oliveira, M.L., Rufino, I.A.A., Cunha, J.E.D.B.L., Vasconcelos, R.S., de Brito, H.C.: Urban growth dynamics based on surface Albedo changes in Petrolina. Brazil. Acta Scientiarum. Technol. **42**, e46270 (2020)
41. Hou, M., Hu, Y., He, Y.: Modifications in vegetation cover and surface albedo during rapid urbanization: a case study from South China. Environ. Earth Sci. **72**, 1659–1666 (2014)
42. Son, N.T., Chen, C.F., Chen, C.R., Chang, L.Y., Thanh, B.X.: Urban growth mapping from Landsat data using linear mixture model in Ho Chi Minh city. Vietnam. J. Appl. Remote Sens. **6**(1), 063543 (2012)
43. Allen, R.G., Tasumi, M., Trezza, R.: Satellite-based energy balance for mapping evapotranspiration with internalized calibration (METRIC)—Model. J. Irrig. Drain. Eng. **133**(4), 380–394 (2007)
44. Weng, Q.: Remote sensing of impervious surfaces in the urban areas: requirements, methods, and trends. Remote Sens. Environ. **117**, 34–49 (2012)
45. Figorito, B., Mancini, F., Novelli, A., Tarantino, E.: Monitoring land cover changes at watershed scale using LANDSAT imagery. Score@ Poliba (2014)
46. Tarantino, E., Figorito, B., Caprioli, M.: Comparison of radiometric normalization methods on LANDSAT ETM+ and ASTER data. Bollettino di Geodesia e Scienze Affini **67**(2), 89–106 (2008)
47. Capolupo, A., Monterisi, C., Barletta, C., Tarantino, E.: Google earth engine for land surface albedo estimation: comparison among different algorithms. In: Proceedings of SPIE, vol. 11856, Remote Sensing for Agriculture, Ecosystems, and Hydrology XXIII, p. 118560F. International Society for Optics and Photonics (2021)
48. Capolupo, A., Monterisi, C., Saponaro, M., Tarantino, E.: Multi-temporal analysis of land cover changes using Landsat data through Google earth engine platform. In: Proceedings of SPIE, vol. 11524, Eighth International Conference on Remote Sensing and Geoinformation of the Environment (RSCy2020), p. 1152419 International Society for Optics and Photonics (2020)